BIOCHEMISTRY
including biophysical chemistry & molecular biology

Article

pubs.acs.org/biochemistry

Secondary and Tertiary Structure of Bacteriorhodopsin in the SDS Denatured State

Venkatramanan Krishnamani,[†,§] Balachandra G. Hegde,[‡] Ralf Langen,[‡] and Janos K. Lanyi*[,†]

[†]Department of Physiology and Biophysics, University of California, Irvine, Irvine, California 92697, United States
[‡]Zilkha Neurogenetic Institute, University of Southern California, Los Angeles, California 90033, United States

Supporting Information

ABSTRACT: We characterized the structure of partially unfolded bacteriorhodopsin in sodium dodecyl sulfate (SDS) micelles and compared it with its *in vitro* refolded structure after reconstitution with dimyristoylphosphatidylcholine/3-[(3-cholamidopropyl)dimethylammonio]-1-propanesulfonate (DMPC/CHAPS). Intrahelical and interhelical distances were mapped in the protein using strategically located spin-label pairs at helical ends, assayed by pulsed electron paramagnetic resonance spectroscopy (double electron−electron spin resonance, DEER). We find that in SDS the intrahelical end-to-end distances exhibit broad distributions, suggesting a heterogeneous ensemble of conformations with differing secondary structures. Nevertheless, a majority of the denatured population retains end-to-end distances similar to those in the native state. In contrast, the observed greatly increased interhelical distances, in addition to their very broad distributions, suggest that in the SDS micelles very little of the native tertiary structure remains.

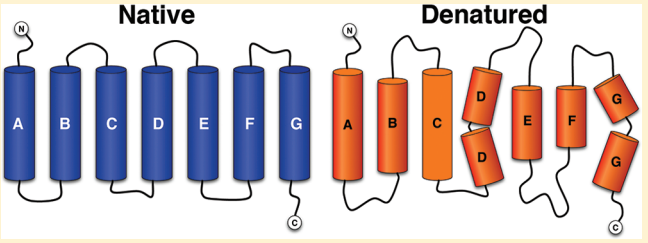

It was established nearly half a century ago by Levinthal[1] that proteins could not possibly fold by a random search of conformational space. As a consequence, there must be well-defined folding pathways by which proteins assemble into their native folds. Studies to understand this pathway are almost always initialized from the denatured state ensemble of the protein. Unfortunately, there is limited structural information about this ensemble state, unlike the native, fully folded structural state. It was shown that the simplified random coil model developed by Flory[2] is not valid for denatured polypeptide chains.[3] Further, experiments[4] and simulations[5] suggest that in the denatured state there is a bias toward native structure. Theoretical calculations have emphasized the importance of this initial denatured ensemble in regulating the folding mechanism.[6] Various groups have investigated the denatured state using NMR,[7,8] but the task of characterizing the structure of the denatured ensemble of proteins is made extremely difficult by its structural disorder.

BR is a small heptahelical protein that functions as a light-driven retinal-based proton pump.[9,10] Membrane proteins like BR are embedded in the lipid bilayer, and once stripped from their native hydrophobic membrane environment, e.g., in aggressive detergents, they partly or fully unfold and/or form aggregates. On the other hand, denaturants that completely destroy the structure of most soluble proteins have little effect. BR is resistant to 8 M guanidinium chloride,[11] and only trifluoroethanoic acid or 88% formic acid transforms the protein to a random coil.

A well-described reversible *in vitro* refolding procedure has been established for BR.[12] Numerous studies to follow the refolding kinetics have been carried out based on this procedure.[13−24] We attempted to resolve the details of this refolding process elsewhere.[25] Since the refolding kinetics commence from the SDS denatured equilibrium state, it is essential to describe and interpret the structural changes observed in its refolding with respect to any remaining secondary or tertiary structure.

Traditional methods like solution NMR for studying disorderly systems have not been successful because of the large system size of denaturing micelles. Estimates of the extent of unfolding by different methods do not seem to agree. The remaining helical content of the protein from CD spectra in SDS micelles yielded nearly half of the original value.[26] However, it was shown that binding of eight SDS molecules decreases the extinction coefficient of bovine serum albumin at 220 nm by 9000 M^{-1} cm^{-1}.[27] Thus, the CD estimation of helical content might not be accurate in detergent micelles.

Deuterium/hydrogen exchange suggested extensive unfolding of the helices.[28] Photo-oxidation labeling of methionines in the whole protein revealed extensive unfolding of helices A and D but not the other helices.[29] On the other hand, the structure of a fragment (helices A plus B) in SDS micelles using NMR revealed a higher degree of structural order than expected, with almost native-like α-helical content for these segments.[30,31] The NMR study also demonstrated that the two-helix fragment of BR in SDS micelles showed no NOE interaction, suggesting loss of tertiary contacts between the helices.[31] Separation of transmembrane helices was also observed in the IR spectra of BR in SDS.[32]

Received: November 30, 2011
Revised: January 11, 2012
Published: January 12, 2012

In this study we employ DEER spectroscopy to probe the distances between spin-labeled sites located at strategic locations to investigate secondary and tertiary structure. Distance measurements using DEER[33] commonly detect interspin distances in the range 15−60 Å, in contrast to the <20 Å range of the continuous wave dipolar interaction method.[34] DEER is thus suitable for monitoring the distance between two spin-labels at the ends of each of the transmembrane helices, which are separated by approximately 30−35 Å. Interspin distances between six separate double spin-labeled samples were measured for determination of intrahelical distances and eight samples for interhelical distance separations (Tables 1 and 2).

Table 1. Summary of Intrahelix Distance Distributions Obtained from DEER

helix	spin-labels	Cβ−Cβ distance (Å)	denatured state DEER distance (Å) (fwhm[a])	regenerated state DEER distance (Å) (fwhm)
A	E9CR1/V29CR1	30	34 (23)	34 (6)
B	K40CR1/G63CR1	34	37 (16)	33 (4)
D	Q105CR1/A126CR1	31	31 (22)	35 (6)
E	S132CR1/F154CR1	33	38 (16)	31 (8)
F	E166CR1/L190CR1	37	39 (21)	44 (16)
G	L201CR1/S226CR1	36	31 (25)	37 (6)

[a]fwhm is full width at half-maximal amplitude.

Table 2. Summary of Interhelix Distance Distributions Obtained from DEER

helix	spin-labels	Cβ−Cβ distance (Å)	denatured state DEER distance (Å) (fwhm[a])
A−C	F27CR1/L100CR1	17	30 (24)
A−F	F27CR1/T170CR1	16	43 (23)
B−E	D38CR1/F156CR1	18	36 (18)
B−F	F42CR1/V167CR1	11	38 (19)
C−F	A103CR1/M163CR1	11	40 (20)
C−G	A103CR1/G231CR1	16	35 (20)
E−G	F156CR1/I222CR1	18	39 (18)
F−G	V167CR1/I222CR1	13	41 (16)

[a]fwhm is full-width at half-maximal amplitude.

Intrahelical distances were measured in the native state (the N state) and in two equilibrium ensemble states: the partially denatured state in SDS micelles (the D-state) and the regenerated state in DMPC/CHAPS micelles (the R-state). Since the Cβ−Cβ distance from the crystal structure and thus of the R-state of the interhelical distance pairs is smaller than the lower detectable limit of the DEER distance range, and since we have previously addressed the regenerated state,[25] interhelical distances in this paper were measured in the partially denatured state only.

A change in the interspin distance of a pair of labels on the ends of a helix (intrahelical) in the different structural states will reflect changes in the overall secondary structure along the helix. Distance change between spin-labels located on two separate helices (interhelical) would reflect a tertiary structural modification.

The possible labeling sites for both interhelical and intrahelical distances were limited. They were chosen such that they were located at the ends of the helices to ensure efficient labeling, as the labeling reaction was carried out for all samples in the membrane embedded N-state. Additionally, attachment sites were selected such that the side chain of the spin-label faced the lipid bilayer; this ensured minimal distance differences due to spin-label orientation. At some locations these strategies had to be compromised to allow for adequate protein expression of the double-cysteine mutants. It should be noted that because of the motion and the extended conformation of the spin-label side-chains, the crystal structure distances between the labeling positions (Cβ−Cβ) listed in Tables 1 and 2 are only approximations of the true interspin distances.

MATERIALS AND METHODS

Mutagenesis and Protein Expression. Cysteines were introduced into BR, which otherwise contains no cysteine, with a well-established homologous expression system.[35] The desired residue change was introduced into a synthetic oligomer primer, 20−30 nucleotides in length, custom-made by Integrated DNA Technologies, Inc. The template DNA pBA2 containing the bop gene (bacterioopsin) was generously provided by M. P. Krebs. The bop gene segment was mutated at specific sites to incorporate a cysteine residue, using a commercially available PCR site-directed mutagenesis kit under the brand name Quikchange XL from Agilent (Santa Clara, CA). The PCR products were digested using restriction endonuclease Dpn1 to remove traces of the original template. The resulting plasmids containing ampR (ampicillin resistance gene) were transformed and proliferated in the host *Escherichia coli* on a nutrient agar plate at 37 °C in the presence of the antibiotic ampicillin. Subsequently, the plasmids were extracted, purified, and sequenced to confirm the inclusion of the desired mutation.

The purified plasmid pBA2 shuttle vector with the mutated bop gene was then transformed into a modified *Halobacterium salinarum* host, MPK409, also kindly provided by M. P. Krebs. In the MPK409 host cells, the native 5-fluororotic acid sensitivity gene *ura*3 is deleted and substituted with an intact *ura*3 gene insertion within the bop (bacterioopsin) gene segment in the *Halobacterium salinarum* chromosome.[36,37] The bop gene in the shuttle vector pBA2 contains the desired mutation, and the mevR gene is used to select for the successful integrants in MPK409 transformants.[35,38] The recombinants were selected using a two-step selection procedure using first mevinolin resistance and then 5-fluororotic acid resistance.

The *Halobacterium* cells thus obtained were cultured in 400 mL complete medium for a day under aerobic conditions in a 2 L culture flask at 38 °C to bring the cell count to a sufficient number for efficient expression of the protein. Following this, the culture flask was filled up to 2 L with Rich Medium[39] and cultured for an additional 4 days at 40 °C under semi-anaerobic conditions for BR purple membrane expression. One of the planned double mutants corresponding to helix C failed to express in the *H. salinarum* expression system. The cysteine mutants for the intrahelical and interhelical distance measurements are shown in Figures 1 and 2, respectively.

Protein Purification. Purple membranes were isolated using a procedure established by Oesterhelt et al.[39] Briefly, the *H. salinarum* cells were resuspended in 4 M NaCl and treated with DNase I for 1 h to digest the genomic DNA. The suspension was transferred to 10 000 MW cutoff dialysis bags and dialyzed at 4 °C against distilled water overnight. All cell membranes other than purple membrane disintegrate. The purple membrane, which contains only BR and lipid, was further purified by series of centrifugation and washing steps and recovered by centrifugation from a 40−60% sucrose gradient.

dx.doi.org/10.1021/bi201769z | *Biochemistry* 2012, 51, 1051−1060

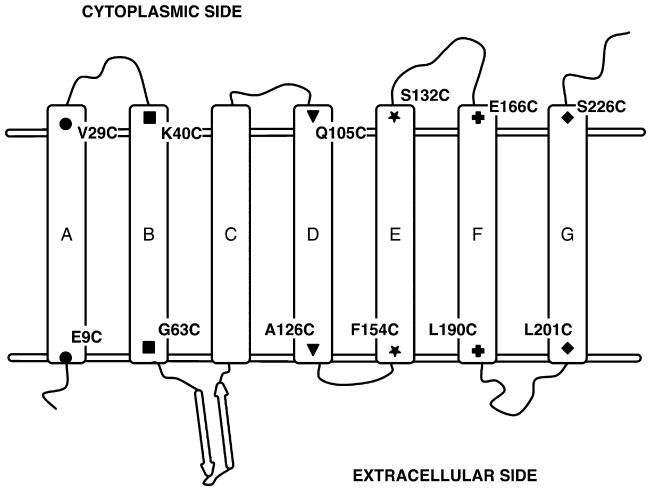

Figure 1. Topology diagram showing the locations of the cysteine mutations designed to measure intrahelical distances in denatured and regenerated state of BR. The locations for each pair of double mutants are represented with the same bold symbol. The horizontal double lines approximate the surface of the lipid bilayer.

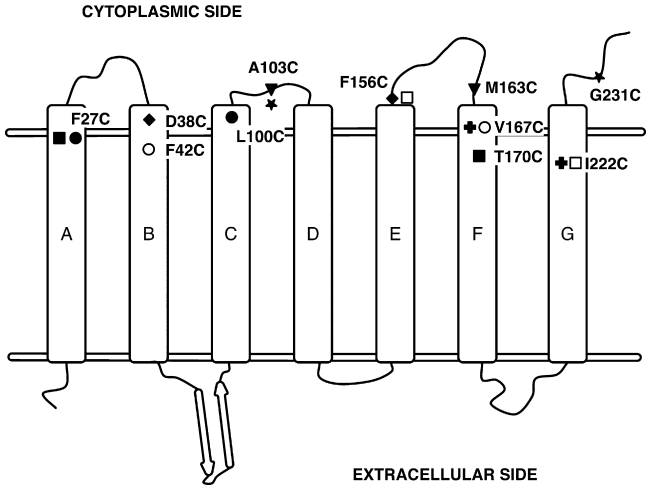

Figure 2. Topology diagram showing the locations of the cysteine mutations designed to measure interhelical distances in denatured state of BR. The locations for each pair of double mutants are represented as the same bold or open symbol. The horizontal double lines approximate the surface of the lipid bilayer.

Spin-Labeling. The labeling reaction was carried out in the purple membrane suspension. Before adding the MTSL reagent for labeling the engineered cysteines, the cysteine residues were reduced by incubating the samples in excess DTT for 30 min. The reducing agent was then removed by four sequential 50× dilutions with 100 mM sodium phosphate buffer (pH 6.5) followed by centrifugation and resuspension of the membranes. After the washing procedure, a 10× molar excess of MTSL was added and incubated at room temperature for 24 h. Excess label was then removed by four centrifugation steps of 50× dilution each with 100 mM sodium phosphate buffer (pH 6.5). All labeling sites were chosen to be at the ends of the helices, where the SH groups of cysteines were accessible. We found that labels at several otherwise desired locations were not accessible to the label, even in the presence of DMSO, used in other reports to label internal locations in BR.[40−42]

***In Vitro* Refolding.** In order to increase the signal-to-noise ratio of the ESR spectrum, the protein concentration of the denatured samples were 10-fold greater, at ca. 100 μM, than in earlier reported refolding experiments to produce the D-state.[11,13,16,26,43,44] The purple membrane was solubilized by adding 2% SDS in pH 6.5 phosphate buffer, maintaining the 1:400 SDS/protein molar ratio of the previously established denaturing conditions.[11,13] Under the renaturing conditions used by the other groups, the chromophore recovery we measured was the same as earlier reported (Supporting Information). However, the concentration of the DMPC/CHAPS could not be scaled up in our experiments to give the same detergent/lipid and lipid/protein ratios because the viscosity would have been unacceptably high. Regeneration that produced the R-state was by adding an equal volume of DMPC/CHAPS micelle suspension (pH 6.5), with the concentration scaled up only 2.5 times (5% DMPC/5% CHAPS) rather than as described elsewhere.[11,13,14,26] At this DMPC/CHAPS concentration, the modified refolding procedure yielded 40−60% chromophore reconstitution, as opposed to the 70−90% previously observed.[13,14] The reconstitution yields were somewhat lower in the cysteine mutants than in the wild-type protein (Supporting Information). It appears that it was this and the lower DMPC/CHAPS to protein ratio that hindered chromophore regeneration. Unlike the yields, the rate constants for chromophore regeneration reported by Khorana, Booth, and co-workers[13,14,26] were reproduced in at the changed protein concentrations (data not shown).

Pulsed EPR−Double Electron−Electron Resonance (DEER). These experiments were performed on a Bruker Elexsys E580 X-band pulse EPR spectrometer fitted with a 3 mm split ring (MS-3) resonator, a continuous-flow helium cryostat (CF935, Oxford Instruments), and a temperature controller (ITC503S, Oxford Instruments). Samples (~90 μM denatured BR sample, ~45 μM regenerated BR sample) were flash-frozen in the presence of 15% glycerol, and data were acquired at 78 K. The pump frequency for the pulsed measurement was set to the maximum of the central absorption peak of the nitroxide spin-label spectrum, and the observer frequency was set to the maximum of the low field absorption peak. A pump frequency pulse of 32 ns was applied to the samples with a 16 and 32 ns pulse width for the observer pulse. A two-step phase cycle was applied to eliminate unwanted echoes. The time for dipolar evolution decay time base was limited to a maximum of 2.4 μs to obtain the optimal signal-to-noise ratio and the ensemble of distances being measured. The dipolar time evolution data were analyzed using DEERAnalysis2010 and MATLAB software packages.[45] The data were fit using single Gaussian peak implemented in the software package.

Although dominated by the desired intramolecular distances, DEER signals in general have some additional contributions from intermolecular interactions. Previous work has shown that this background can be subtracted and that the shape of the background signal depends on whether spin-labeled proteins engage in intermolecular interactions within two or three dimensions.[45] Unlike membrane proteins within bilayers, detergent solubilized proteins are arranged in three dimensions with respect to each other. We therefore used the 3-D background subtraction model, and the baseline assumption was additional verified by comparing signals with different time evolution times (1−2.4 μs). The background contribution was subtracted using a three-dimensional model for SDS micelles denatured BR samples. Since DMPC/CHAPS mixture forms

dx.doi.org/10.1021/bi201769z | *Biochemistry* 2012, 51, 1051−1060

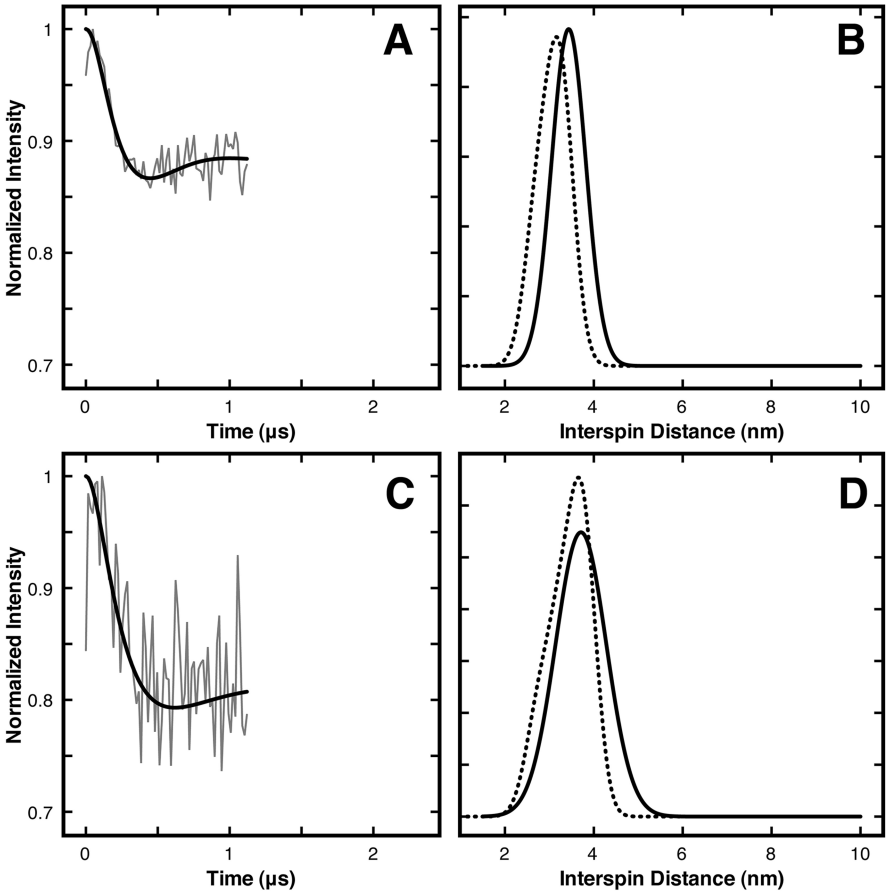

Figure 3. Intrahelical end-to-end distance measurement for helix B (A and B) and helix F (C and D) in the native state (bold lines B and D) compared to the distance distribution obtained from crystal structure (dashed lines in B and D). The crystal structure distance distribution was generated by a weighted Gaussian with a width of 5 Å for each pair of spin-label location in a two-dimensional array of BR with a distance cutoff determined by the DEER detectable distance range (15−60 Å). The distances are measured between the Cβ atom locations from the crystal structure.

bilayer disk (bicelle),[46] a two-dimensional model was used for background subtraction of regenerated samples. The measurements for label pairs 40−63 and 166−190 were performed in duplicate.

Polymer Model. End-to-end distance distribution of a random coil with a chain length of each helix was calculated separately using a wormlike chain (WLC) polymer model.[47] This distribution was used as a comparison to the experimentally obtained DEER end-to-end distance distributions. For a persistence length l_p and contour length l_c of the polymer chain, the probability distribution of end-to-end distance $P(R)$ for WLC is accurately given by[48,49]

$$P(R) = 4\pi R^2\left(\frac{3}{4\pi l_p l_c}\right)^{3/2}\exp\left(\frac{-3R^2}{4l_p l_c}\right)\left(1 - \frac{5l_p}{4l_c} + \frac{2R^2}{{l_c}^2} - \frac{33R^4}{80l_p{l_c}^3} - \frac{79{l_p}^2}{160{l_c}^2} - \frac{329R^2 l_p}{120{l_c}^3} + \frac{6799R^4}{1600{l_c}^4} - \frac{3441R^6}{2800l_p{l_c}^5} + \frac{1089R^8}{12800{l_p}^2{l_c}^6}\right) \quad (1)$$

The $C_\alpha-C_\alpha$ distance of b = 0.38 nm was used for calculating contour length l_c of each sample using $l_c = Lb$. L is the number of amino acids between the two spin-labels. The persistence length l_p is roughly the measure of the length scale over which a polymer remains rigid. The value of l_p = 0.4 nm was assumed, as protein loop fragments weakly tethered at its ends behaves like wormlike chain with a persistence length of 0.4 nm.[50]

RESULTS

The spin-to-spin distances in doubly labeled BR samples (Figures 1 and 2) were obtained from four-pulse DEER experiments using the time evolution of the a spin-echo pulse.[33] The frequency of oscillation of the signal decay directly measures the interspin distance, with higher frequency oscillations corresponding to shorter distances. Fitting these oscillations produced estimates of the distribution of distances in the heterogeneous ensembles that constitute the D (denatured) and R (renatured) states.

To evaluate the reliability of distances from the pulsed ESR measurements, helix end-to-end distances of BR in the native state (N-state) were measured (Figure 3). Unlike in the R-state,[26] BR in membrane patches is arranged as trimers in a two-dimensional crystalline lattice.[51,52] The distance distributions obtained after subtraction of the background of intermolecular spin−spin interactions (see Materials and Methods) for helices B and F (Figures 3B and 3D, bold lines) were only slightly shifted (1−3 Å) from the expected large single peak of distances calculated (Figures 3B and 3D, dotted lines) from crystal structure (using PDB: 1C3W). This is as expected when considering the rotamers and the orientation of spin-labels that contribute to the measured distance. The width of the observed distribution corresponded closely with the calculated distribution. The calculation was performed with the assumption that the spin-label rotamers add ±5 Å to the C$\beta-$Cβ distance

dx.doi.org/10.1021/bi201769z | *Biochemistry* 2012, 51, 1051−1060

obtained from the crystal structure. For helices A, D, E, and G, after background subtraction, the signal could not be distinguished from the baseline (not shown). This large background is attributed to the numerous additional intermolecular distances between spin-label pairs in these cases, as a result of the closely packed monomers of BR in the native state. Because of the complexity in the analysis of distance distributions in the N-state and since not all N-state distance distributions could be obtained, only the D-state and R-state will be discussed in this paper.

The end-to-end distances measured for all labeled pairs are between the nitroxide moieties located at the end of the spin-label's side chain. In addition to helix length the measured distance has contributions from relative orientations of the spin-label pair and backbone flexibility. Thus, the Cβ−Cβ distance of the label locations from crystal structure should provide only an approximate measure of the interlabel distances, and the crystal distances are shown only for reference.

Secondary Structure. Intrahelical end-to-end distances were determined to monitor the secondary structure of the helical segments in the D- and R-state. The peaks of these end-to-end distance distributions in the D-state and R-state are listed in Table 1, along with the corresponding Cβ−Cβ distances in the crystal structure. The intrahelical distance distributions for the D-state are shown in Figure 4, (right panels) A, C, E, G, I, and K, and those for the corresponding R-state are in Figure 4, (right panels) B, D, F, H, J, and L. The raw data of DEER measurements and their fits are shown on the left of each distance distribution graph.

Overall, the peak of the D-state distance distribution varies between 0 and 7 Å when compared to the corresponding R-state. The distribution width of end-to-end distance of the helices in R-state is much narrower (width 4−8 Å) than in the D-state (width 16−25 Å). Helix F, like the rest of the measured helices, has a wide distance distribution in the D-state but displays a remarkably wide distance distribution in the R-state also (Figure 4J). The data strongly indicate the re-establishment of the secondary structure in the R-state in all helices examined (Figure 4 B,D,F,H,L), but not for helix F (Figure 4J). The inconsistency of helix F will be discussed in below. The distance of the majority of the conformational population in the R-state returns to the crystal structure estimates within the expected error margin. The remaining distance spread of each R-state distribution is most likely due to the various rotameric states of the spin-label, implying that the helices have a well-defined secondary structure with a rigid backbone.

The broader distance distribution of the D-state suggests conformational heterogeneity of a more flexible backbone, from at least partial unraveling of the helices. The mean end-to-end distances changed too little to suggest extensive unfolding, however. As a point of reference in understanding the degree of unfolding in the helices, end-to-end distance distributions of a complete random coil using a wormlike chain model with weakly tethered ends were calculated (Figure 4A,C,E,G,I,K, dotted lines). The WLC model has been successfully applied to describe end-to-end distance distributions of protein loops.[50,53] It should be noted that this model does not take into account the fact that the protein is in a micelle. For a peptide in a completely random coil conformation the WLC model predicts shorter mean distances than observed in the D-state (Figure 4). The clear contrast between the two distributions and a larger peak distance of the D-state suggest that the helices are not in a random coil conformation in the SDS micelles, and a significant population of the D-state ensemble of all the six helices retains some helical structure. An attempt to fit the DEER distance distribution to the WLC model did not yield a statistically significant fit (not shown). In the following sections, we discuss the results for each helix.

Helix A shows no deviation in peak distance in SDS micelles and DMPC/CHAPS micelles (Figure 4A,B, right panels). In the latter, R-state, however, the distribution is significantly narrower. Assuming that the range of conformations of the spin-label is unchanged between the two states, this suggests that a significant population of helix A in the ensemble becomes more flexible in the D-state (distances on either side of the mean). This is possibly due to partial unfolding of the helix. Nevertheless, the majority of the population in the D-state exhibits peak distances similar to the R-state. This is consistent with a fully folded helix as a major component in the D-state of helix A, consistent with previous NMR experiments, which showed that helix-A fragment remains unchanged in helical content in SDS micelles when compared to its native state.[30,31]

Along with the common observed trend of decreasing distribution width of the DEER distance distributions, helices B and E show decreases of the peak of distance distribution upon transition from the D-state to the R-state (Figure 4C,D,G,H). This suggests that some regions of these helices are frayed in the SDS micelles, leading to increase in the distance between the spin-labels of the major population in the D-state. The regions that have so unraveled in SDS micelles can be identified only with experiments with more spin-labels, but we tried to wobtain some clues with molecular dynamics simulations [accompanying paper, Krishnamani and Lanyi, *Biochemistry*, 2012].

In contrast, helices D, F, and G exhibit increases of peak distance between the D-state and the R-state (Figure 4E,F,I−L). A smaller helix end-to-end distance of the major population in the D-state can be visualized by kinks/bends induced and stabilized by SDS. For example, the unraveling of a few residues at the center of the helix can cause such kinking of the helix. We see evidence of such kink/bend in helices D, F, and G in our molecular dynamics simulations [accompanying paper, Krishnamani and Lanyi, *Biochemistry*, 2012]. The behavior of helix F is unlike the others. The mean distance distribution in the R-state remains increased by 10 Å from the distance predicted from the crystal structure (Figure 4, panel J). The possible reasons are discussed further below.

A distance distribution for helix C could not be obtained due to inability to express the appropriate mutant protein in our expression system.

Tertiary Structure. The tertiary structure of BR in the D-state was mapped from interhelical distances. The interhelical distances measured in the denatured state are summarized in Table 2. The raw data of DEER measurements and their fits are shown on the left of the distance distribution for each spin pair (Figure 5). We do not expect a complete random distribution of interhelical distances as the helices are tethered to each other in the protein chain, and the need to be confined inside the micelles will impose restrictions to the separation of helices with hydrophobic side-chains.

We observe a broad distribution of distances for all the interhelical distance pairs in the denatured state (16−24 Å), suggesting considerable heterogeneity in the denatured ensemble (Table 2 and Figure 5, right panels). The peaks of the distance distributions obtained for all interhelical spin pairs in the D-state are shifted to greater distances, by at least a

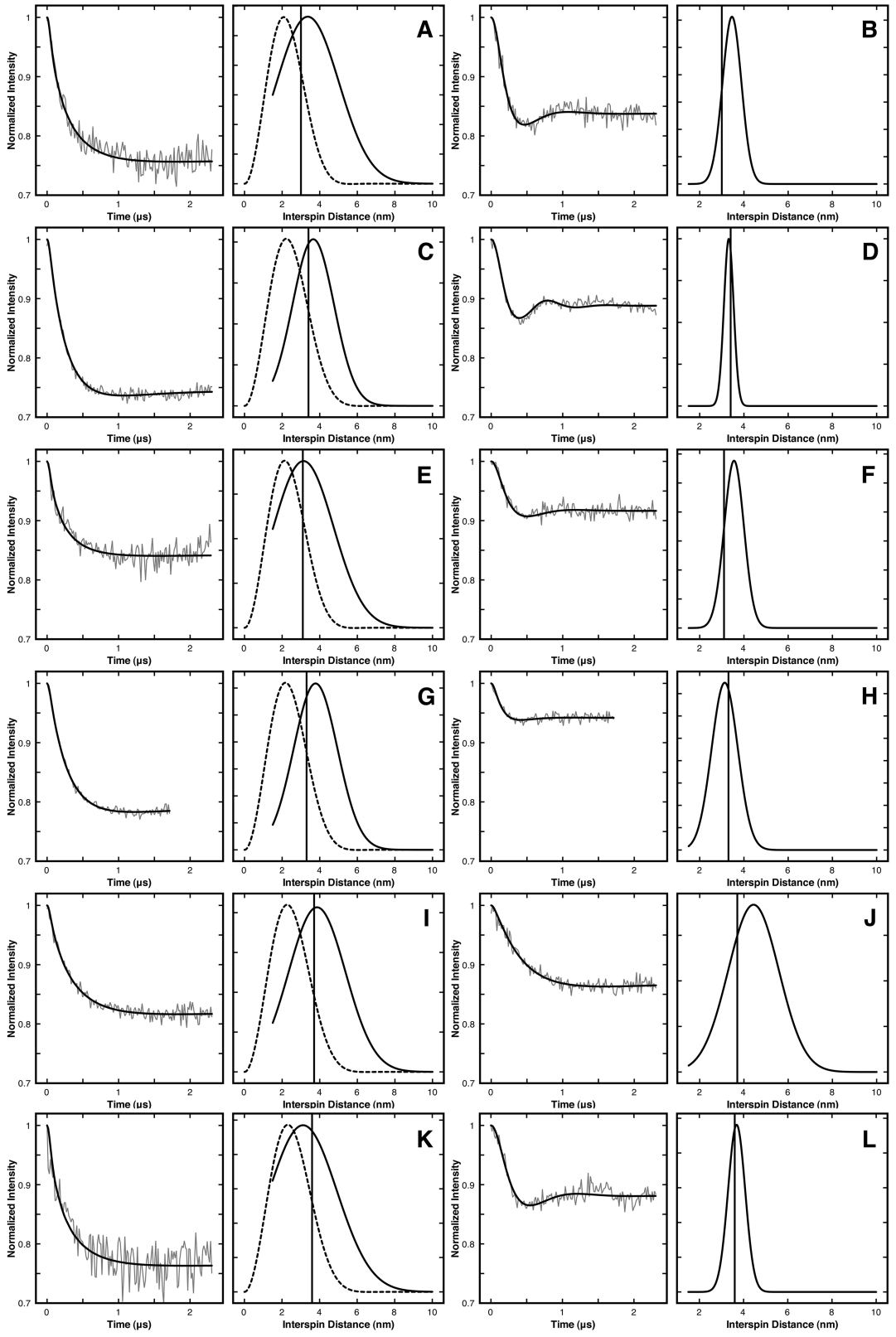

Figure 4. Intrahelical distance distributions of the conformational ensembles of the denatured state and the regenerated state of helix A (A and B), helix B (C and D), helix D (E and F), helix E (G and H), helix F (I and J), and helix G (K and L) from DEER experiments. The corresponding time domain dipolar evolution spectra (gray lines), along with the best fit (black solid lines) are shown on the left of each labeled panel. The vertical lines in the distance distribution curves indicate the Cβ−Cβ distance of the labeled residue positions estimated from the crystal structure. The theoretically modeled distance distributions, based on a wormlike chain (eq 1), are shown as broken lines. l_p = 0.4 nm[50,53] and $l_c = bL$, where b = 0.38 nm and L = number of residues between the two spin-labels.

dx.doi.org/10.1021/bi201769z | *Biochemistry* 2012, 51, 1051−1060

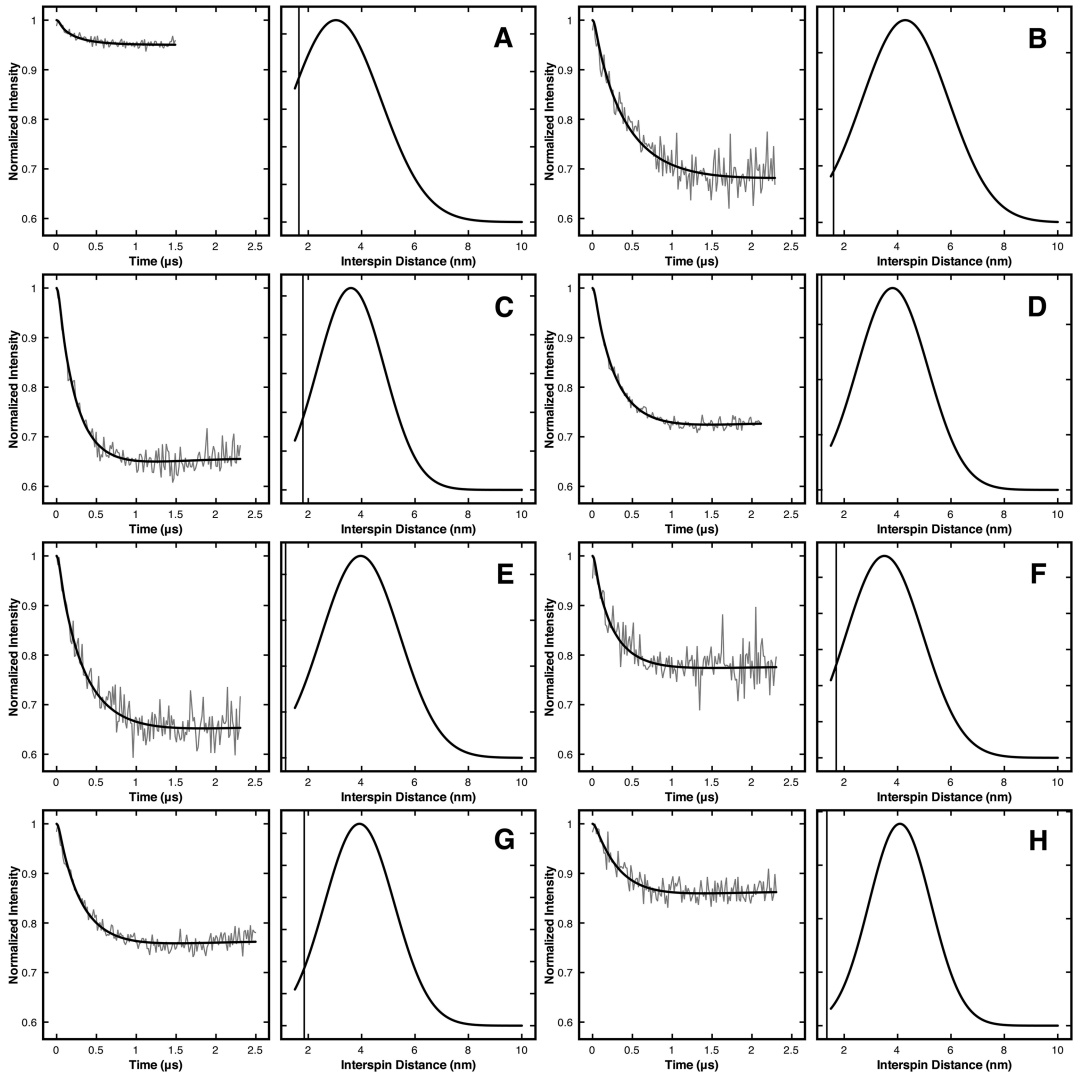

Figure 5. Interhelical distance distributions in the conformational ensembles of helices A and C (A), helices A and F (B), helices B and E (C) and helices B and F (D), helices C and F (E), helices C and G (F), helices E and G (G), and helices F and G (H) in the denatured state. The locations of the labels are illustrated in Figure 2. The corresponding time domain dipolar evolution spectra (gray lines), along with the best fit (black solid lines) are shown in the immediate left of each labeled panel. The vertical lines in the distance distributions indicate the Cβ−Cβ distance of the labeled residue positions estimated from the crystal structure.

factor of 2, from their corresponding crystal structure estimates (Table 2).

The distance distribution obtained for tertiary structure has contributions from partial disruption of secondary structure, backbone fluctuations, spin-label orientations, and the loss of tertiary contacts. This complicates a rigorous analysis of the distance distribution obtained. Nevertheless, a large shift in the distance peak and heterogeneity of the interhelical distance distribution most likely suggests extensive loss of tertiary structure in the D-state.

DISCUSSION

Earlier experiments had indicated that a considerable amount of overall helicity (~50% of the original extent) might be retained in the SDS micelles,[18] but it was unclear which helices or what segments in the helices were preserved. We observe that in SDS micelles the helices display a broad distribution of distances but the peak of the distance distributions are relatively unchanged from the predicted distances from crystal structure (Figure 3A,C,E,G,I,K, right panels). This suggests structural heterogeneity with the major population, but with much of the original helical content retained. In contrast, the interhelical distance peaks (measuring tertiary structure) show significant shifts to higher distances as well as a higher degree of heterogeneity in the denatured ensemble.

From our results we conclude that, it is the heterogeneous ensemble of disrupted and intact segments in each of the six helices measured that accounts for the observed reduction in the helical content in SDS micelles, rather than a single conformation. A clear difference of the D-state distance distributions from the predictions of the WLC model provides a high confidence in proposing the absence of an extensive random coiled structure in SDS micelles.

The presence of transmembrane segments surrounded by SDS molecules in a micelle seems to provide an environment that protects and retains α-helical structure, at least partially, from the results above. Such stabilizing effect of SDS micelles could be seen in TM helices of Saposin C and glycophorin A.[54,55] In a molecular dynamics study,[56] the unfolded state of a soluble

dx.doi.org/10.1021/bi201769z | *Biochemistry* 2012, 51, 1051−1060

α-helical peptide in water was shown to have a range of conformations from fully unfolded coil to small helical segments interspersed with turn regions, in an equilibrium. As a conservative estimate based on the width of DEER distance distribution, the helicity lost in BR would be equivalent to no more than about 2−8 residues in any of the six helices we studied (A, B, D, E, F, and G), assuming full stretching of the disrupted residues limited only by the length of the peptide bond between residues.

Pan et al. recently presented methionine photolabeling of BR in SDS micelles that showed that helices A (and D) are largely unfolded.[28,29] Helices B, C, E, F, and G, in turn, have been proposed to partially intact with the methionine side chain and protect them from solvent exposure, either by being buried in the SDS micelles or by retention of an intact protein core. Thus, the lack or the presence of solvent exposure of methionine does not necessarily provide evidence of unfolding. It is easy to imagine a local area surrounding the methionine being protected by SDS molecules or partial exposure of the methionine side chain to the solvent in a dynamic system. We observe evidence of partial unfolding of all the helices in the D-state with a heterogeneous structural state.

Heterogeneity can be interpreted as equilibrium between multiple equal energy conformations in an energy landscape. These equilibrium structural ensembles present themselves as various DEER distance distributions. Addition of lipid (DMPC) and another, milder detergent (CHAPS) would shift the equilibrium toward refolding and restoration of native structure. In such a refolding reaction scheme the helices are reestablished rapidly (in <100−140 ms) and then follow a kinetic pathway with intermediate states depending upon the energy barriers of refolding of the helices into a native-like bundle.[25]

The transition from one equilibrium-unfolded state to another can be triggered by a combination of various events. Helix nucleation in the extended partially unfolded helix can rapidly initiate assumption of a folded helical structure due to the highly cooperative nature of helix formation.[57] Conversely, destabilization of hydrogen bonds in a helical structure can occur by competition with water molecules or the head groups of SDS molecules, unfolding a local region. The ease of transition or rates of equilibrium transitions determines the population of these states.

The variation in structural changes observed between the BR helices has to originate from the residue sequences of the transmembrane segments and sequence-dependent interaction with its environment. The accompanying paper [Krishnamani and Lanyi, *Biochemistry*, 2012] discusses the sequence dependence of structural perturbation of the helices in SDS micelles using molecular dynamics simulation.

The DEER distance distributions for the R-state of BR shows apparent complete recovery of the secondary structures of helices A, B, D, E, and G, although not F. Yet under our renaturation conditions the retinal-dependent chromophore is not completely regenerated in the R-state (40−60%). Thus, recovery of the helices does not ensure recovery of the chromophore. Possibly, the native tertiary structure is assumed only when helix F recovers also. Alternatively, regeneration of helix F may be necessary for the binding of retinal. Helix F carries the three aromatic residues, Trp-182, Tyr-185, and Trp-189, that define the binding site for the retinal polyene chain and the β−ionone ring.[58] It seems very unlikely that chromophore recovery could occur without a folded helix F that is docked to its right place in the heptahelical bundle. We conclude that the cause of partial recovery of the chromophore must be the partial refolding of helix F.

The reason for poor regeneration of helix F might be in the lipid used for the reconstitution. Archaebacterial lipids are phosphatidyl glycerols with ether linkage to isoprenoid alcohols containing 20 and 25 carbon atoms,[59] of which 16 or 20 carbon atoms contribute to the length of the lipid tail. Importantly, since these lipid tails are longer than the 14-carbon atoms long chain of the DMPC in the reconstitution, there is a possibility of hydrophobic mismatch with the transmembrane helices. Given that helix F is the longest helix, it is more likely to be affected by hydrophobic mismatch. Such a mismatch can result in fraying of the hydrophobic regions at the ends of the helices, particularly at the higher detergent/lipid ratio we used, and might be the reason for the increased distances observed for the R-state of helix F. Significantly, it was reported that of all individually synthesized bacteriorhodopsin helices helix F alone did not form an α-helix in lipid bilayers.[60]

In an earlier NMR study of a BR segment that included helices A and B in SDS micelles showed no interproton nuclear Overhauser effect (NOE) between the helices.[31] Since NOE interactions are observed over less than a few angstroms, helical segments A and B that lie adjacent to one another in the native structure must have become separated in the micelles, while the helical structures were largely conserved. NMR studies of Saposin C had shown that this protein adopts an open conformation with an exposed hydrophobic pocket in SDS micelles.[61] In this system it was also observed that SDS displaces hydrophobic protein−protein contacts with detergent−protein contacts. Likewise, crystallographic studies on SDS denatured lysozyme had shown that the detergent molecules intercalate into the hydrophobic core of the protein and "open up" the structure.[62] Our observation that there is loss of most, or even all, tertiary contacts of between helical pairs of BR in SDS micelles is consistent with the above studies.

■ ASSOCIATED CONTENT

Ⓢ Supporting Information

Table S1. This material is available free of charge via the Internet at http://pubs.acs.org.

■ AUTHOR INFORMATION

Corresponding Author

*E-mail: jklanyi@uci.edu; phone: (949) 824-7150, fax: (949) 824-8540.

Present Address

[§]Department of Physics, Carnegie Mellon University, Pittsburgh, PA 15213.

Funding

The authors gratefully acknowledge the National Institutes of Health, Grant 5R37GM029498 to J.K.L., for funding the construction of mutants and the Division of Chemical Sciences, Geosciences, and Biosciences, Office of Basic Energy Sciences of the U.S. Department of Energy, Grant DEFG03-86ER13525 to J.K.L., for funding the ESR experiments.

Notes

The authors declare no competing financial interest.

■ ABBREVIATIONS

BR, bacteriorhodopsin; SDS, sodium dodecyl sulfate; DMPC, dimyristoylphosphatidyl choline; N, D, and R states, native, SDS denatured, and regenerated states of BR; CHAPS, 3-[(3-

cholamidopropyl)dimethylammonio]-1-propanesulfonate; DEER, double electron electron resonance; MTSL, (1-oxyl-2,2,5,5-tetramethylpyrolinyl-3-methyl)methanethiosulfonate; DTT, dithothreitol; WLC, wormlike chain model.

REFERENCES

(1) Levinthal, C. (1968) Are There Pathways for Protein Folding. *J. Chim. Phys. Phys.-Chim. Biol. 65*, 44−45.

(2) Flory, P. J., and Volkenstein, M. (1969) Statistical mechanics of chain molecules. *Biopolymers 8*, 699−700.

(3) Pappu, R. V., Srinivasan, R., and Rose, G. D. (2000) The Flory isolated-pair hypothesis is not valid for polypeptide chains: implications for protein folding. *Proc. Natl. Acad. Sci. U. S. A. 97*, 12565−12570.

(4) Marqusee, S., Robbins, V. H., and Baldwin, R. L. (1989) Unusually stable helix formation in short alanine-based peptides. *Proc. Natl. Acad. Sci. U. S. A. 86*, 5286−5290.

(5) Srinivasan, R., and Rose, G. D. (1999) A physical basis for protein secondary structure. *Proc. Natl. Acad. Sci. U. S. A. 96*, 14258−14263.

(6) Klimov, D. K., and Thirumalai, D. (2005) Symmetric connectivity of secondary structure elements enhances the diversity of folding pathways. *J. Mol. Biol. 353*, 1171−1186.

(7) Dill, K. A., and Shortle, D. (1991) Denatured states of proteins. *Annu. Rev. Biochem. 60*, 795−825.

(8) Shortle, D. R. (1996) Structural analysis of non-native states of proteins by NMR methods. *Curr. Opin. Struct. Biol. 6*, 24−30.

(9) Lanyi, J. K., and Schobert, B. (2003) Mechanism of proton transport in bacteriorhodopsin from crystallographic structures of the K, L, M1, M2, and M2′ intermediates of the photocycle. *J. Mol. Biol. 328*, 439−450.

(10) Haupts, U., Tittor, J., and Oesterhelt, D. (1999) Closing in on bacteriorhodopsin: progress in understanding the molecule. *Annu. Rev. Biophys. Biomol. Struct. 28*, 367−399.

(11) Huang, K. S., Bayley, H., Liao, M. J., London, E., and Khorana, H. G. (1981) Refolding of an integral membrane protein. Denaturation, renaturation, and reconstitution of intact bacteriorhodopsin and two proteolytic fragments. *J. Biol. Chem. 256*, 3802−3809.

(12) Huang, K. S., Bayley, H., and Khorana, H. G. (1980) Delipidation of bacteriorhodopsin and reconstitution with exogenous phospholipid. *Proc. Natl. Acad. Sci. U. S. A. 77*, 323−327.

(13) Booth, P. J., Flitsch, S. L., Stern, L. J., Greenhalgh, D. A., Kim, P. S., and Khorana, H. G. (1995) Intermediates in the folding of the membrane protein bacteriorhodopsin. *Nat. Struct. Biol. 2*, 139−143.

(14) Booth, P. J., Farooq, A., and Flitsch, S. L. (1996) Retinal binding during folding and assembly of the membrane protein bacteriorhodopsin. *Biochemistry 35*, 5902−5909.

(15) Sugiyama, Y., and Mukohata, Y. (1996) Dual roles of DMPC and CHAPS in the refolding of bacterial opsins in vitro. *J Biochem. 119*, 1143−1149.

(16) Booth, P. J. (1997) Folding alpha-helical membrane proteins: kinetic studies on bacteriorhodopsin. *Folding Des. 2*, R85−92.

(17) Booth, P. J., Riley, M. L., Flitsch, S. L., Templer, R. H., Farooq, A., Curran, A. R., Chadborn, N., and Wright, P. (1997) Evidence that bilayer bending rigidity affects membrane protein folding. *Biochemistry 36*, 197−203.

(18) Riley, M. L., Wallace, B. A., Flitsch, S. L., and Booth, P. J. (1997) Slow alpha helix formation during folding of a membrane protein. *Biochemistry 36*, 192−196.

(19) Curran, A. R., Templer, R. H., and Booth, P. J. (1999) Modulation of folding and assembly of the membrane protein bacteriorhodopsin by intermolecular forces within the lipid bilayer. *Biochemistry 38*, 9328−9336.

(20) Lu, H., and Booth, P. J. (2000) The final stages of folding of the membrane protein bacteriorhodopsin occur by kinetically indistinguishable parallel folding paths that are mediated by pH. *J. Mol. Biol. 299*, 233−243.

(21) Allen, S. J., Kim, J. M., Khorana, H. G., Lu, H., and Booth, P. J. (2001) Structure and function in bacteriorhodopsin: the effect of the interhelical loops on the protein folding kinetics. *J. Mol. Biol. 308*, 423−435.

(22) Lu, H., Marti, T., and Booth, P. J. (2001) Proline residues in transmembrane alpha helices affect the folding of bacteriorhodopsin. *J. Mol. Biol. 308*, 437−446.

(23) Compton, E. L., Farmer, N. A., Lorch, M., Mason, J. M., Moreton, K. M., and Booth, P. J. (2006) Kinetics of an individual transmembrane helix during bacteriorhodopsin folding. *J. Mol. Biol. 357*, 325−338.

(24) Pan, Y., Brown, L., and Konermann, L. (2011) Kinetic folding mechanism of an integral membrane protein examined by pulsed oxidative labeling and mass spectrometry. *J. Mol. Biol. 410*, 146−158.

(25) Krishnamani, V., and Lanyi, J. K. (2011) Structural Changes in Bacteriorhodopsin during In Vitro Refolding from a Partially Denatured State. *Biophys. J. 100*, 1559−1567.

(26) London, E., and Khorana, H. G. (1982) Denaturation and renaturation of bacteriorhodopsin in detergents and lipid-detergent mixtures. *J. Biol. Chem. 257*, 7003−7011.

(27) Polet, H., and Steinhardt, J. (1968) Binding-induced alterations in ultraviolet absorption of native serum albumin. *Biochemistry 7*, 1348−1356.

(28) Pan, Y., Brown, L., and Konermann, L. (2011) Hydrogen/deuterium exchange mass spectrometry and optical spectroscopy as complementary tools for studying the structure and dynamics of a membrane protein. *Int. J. Mass Spectrom. 302*, 3−11.

(29) Pan, Y., Brown, L., and Konermann, L. (2010) Site-directed mutagenesis combined with oxidative methionine labeling for probing structural transitions of a membrane protein by mass spectrometry. *J. Am. Soc. Mass Spectrom. 21*, 1947−1956.

(30) Pervushin, K. V., Arseniev, A. S., Kozhich, A. T., and Ivanov, V. T. (1991) Two-dimensional NMR study of the conformation of (34−65)bacterioopsin polypeptide in SDS micelles. *J. Biomol. NMR 1*, 313−322.

(31) Pervushin, K. V., Orekhov, V., Popov, A. I., Musina, L., and Arseniev, A. S. (1994) Three-dimensional structure of (1−71)-bacterioopsin solubilized in methanol/chloroform and SDS micelles determined by 15N-1H heteronuclear NMR spectroscopy. *Eur. J. Biochem. 219*, 571−583.

(32) Torres, J., Sepulcre, F., and Padros, E. (1995) Conformational changes in bacteriorhodopsin associated with protein-protein interactions: a functional alpha I-alpha II helix switch? *Biochemistry 34*, 16320−16326.

(33) Pannier, M., Veit, S., Godt, A., Jeschke, G., and Spiess, H. W. (2000) Dead-time free measurement of dipole-dipole interactions between electron spins. *J. Magn. Reson. 142*, 331−340.

(34) Rabenstein, M. D., and Shin, Y. K. (1995) Determination of the distance between two spin labels attached to a macromolecule. *Proc. Natl. Acad. Sci. U. S. A. 92*, 8239−8243.

(35) Krebs, M. P., Mollaaghababa, R., and Khorana, H. G. (1993) Gene replacement in Halobacterium halobium and expression of bacteriorhodopsin mutants. *Proc. Natl. Acad. Sci. U. S. A. 90*, 1987−1991.

(36) Krebs, M. P., Hauss, T., Heyn, M. P., Rajbhandary, U. L., and Khorana, H. G. (1991) Expression of the Bacterioopsin Gene in Halobacterium-Halobium Using a Multicopy Plasmid. *Proc. Natl. Acad. Sci. U. S. A. 88*, 859−863.

(37) Peck, R. F., DasSarma, S., and Krebs, M. P. (2000) Homologous gene knockout in the archaeon Halobacterium salinarum with ura3 as a counterselectable marker. *Mol. Microbiol. 35*, 667−676.

(38) Cline, S. W., and Doolittle, W. F. (1987) Efficient transfection of the archaebacterium Halobacterium halobium. *J. Bacteriol. 169*, 1341−1344.

(39) Oesterhelt, D., and Stoeckenius, W. (1974) Isolation of the cell membrane of Halobacterium halobium and its fractionation into red and purple membrane, in *Methods in Enzymology* (Sidney Fleischer, L. P., Ed.) pp 667−678, Academic Press, New York.

(40) Misch, D. W., and Misch, M. S. (1975) Effect of Dimethyl-Sulfoxide on a Lysosomal Membrane. *Ann. N. Y. Acad. Sci. 243*, 54−59.

(41) Aracava, Y., Schreier, S., Phadke, R., Deslauriers, R., and Smith, I. C. P. (1981) Spin Label Reduction Kinetics, a Procedure to Study the Effect of Drugs on Membrane-Permeability - the Effects of Monosodium Urate, Dimethylsulfoxide and Amphotericin-B. *J. Biochem. Biophys. Methods 5*, 83−94.
(42) Steinhoff, H. J., Pfeiffer, M., Rink, T., Burlon, O., Kurz, M., Riesle, J., Heuberger, E., Gerwert, K., and Oesterhelt, D. (1999) Azide reduces the hydrophobic barrier of the bacteriorhodopsin proton channel. *Biophys. J. 76*, 2702−2710.
(43) Allen, S. J., Curran, A. R., Templer, R. H., Meijberg, W., and Booth, P. J. (2004) Folding kinetics of an alpha helical membrane protein in phospholipid bilayer vesicles. *J. Mol. Biol. 342*, 1279−1291.
(44) Curnow, P., and Booth, P. J. (2007) Combined kinetic and thermodynamic analysis of alpha-helical membrane protein unfolding. *Proc. Natl. Acad. Sci. U. S. A. 104*, 18970−18975.
(45) Jeschke, G., Chechik, V., Ionita, P., Godt, A., Zimmermann, H., Banham, J., Timmel, C. R., Hilger, D., and Jung, H. (2006) DeerAnalysis2006 - a comprehensive software package for analyzing pulsed ELDOR data. *Appl. Magn. Reson. 30*, 473−498.
(46) Brouillette, C. G., McMichens, R. B., Stern, L. J., and Khorana, H. G. (1989) Structure and thermal stability of monomeric bacteriorhodopsin in mixed phospholipid/detergent micelles. *Proteins 5*, 38−46.
(47) Kratky, O., and Porod, G. (1949) Rontgenuntersuchung Geloster Fadenmolekule. *Recl. Trav. Chim. Pays-Bas 68*, 1106−1122.
(48) Gobush, W., Yamakawa, H., Stockmay, W. H., and Magee, W. S. (1972) Statistical Mechanics of Wormlike Chains. 1. Asymptotic Behavior. *J. Chem. Phys. 57*, 2839−2842.
(49) Yamakawa, H., and Stockmay, W., H. (1972) Statistical Mechanics of Wormlike Chains. 2. Excluded Volume Effects. *J. Chem. Phys. 57*, 2843−2854.
(50) Zhou, H. X. (2004) Polymer models of protein stability, folding, and interactions. *Biochemistry 43*, 2141−2154.
(51) Blaurock, A. E., and Stoecken., W. (1971) Structure of Purple Membrane. *Nature (London), New Biol. 233*, 152−&.
(52) Henderson, R., and Unwin, P. N. T. (1975) 3-Dimensional Model of Purple Membrane Obtained by Electron-Microscopy. *Nature 257*, 28−32.
(53) Zhou, H. X. (2001) Loops in proteins can be modeled as worm-like chains. *J. Phys. Chem. B 105*, 6763−6766.
(54) Hawkins, C. A., de Alba, E., and Tjandra, N. (2005) Solution structure of human saposin C in a detergent environment. *J. Mol. Biol. 346*, 1381−1392.
(55) Braun, R., Engelman, D. M., and Schulten, K. (2004) Molecular dynamics simulations of micelle formation around dimeric glycophorin A transmembrane helices. *Biophys. J. 87*, 754−763.
(56) Sorin, E. J., and Pande, V. S. (2005) Exploring the helix-coil transition via all-atom equilibrium ensemble simulations. *Biophys. J. 88*, 2472−2493.
(57) Fersht, A. R. (1997) Nucleation mechanisms in protein folding. *Curr. Opin. Struct. Biol. 7*, 3−9.
(58) Luecke, H., Schobert, B., Richter, H. T., Cartailler, J. P., and Lanyi, J. K. (1999) Structure of bacteriorhodopsin at 1.55 A resolution. *J. Mol. Biol. 291*, 899−911.
(59) Derosa, M., Gambacorta, A., and Gliozzi, A. (1986) Structure, Biosynthesis, and Physicochemical Properties of Archaebacterial Lipids. *Microbiol. Rev. 50*, 70−80.
(60) Hunt, J. F., Earnest, T. N., Bousche, O., Kalghatgi, K., Reilly, K., Horvath, C., Rothschild, K. J., and Engelman, D. M. (1997) A biophysical study of integral membrane protein folding. *Biochemistry 36*, 15156−15176.
(61) Hawkins, C. A., de Alba, E., and Tjandra, N. (2005) Solution structure of human saposin C in a detergent environment. *J. Mol. Biol. 346*, 1381−1392.
(62) Yonath, A., Podjarny, A., Honig, B., Sielecki, A., and Traub, W. (1977) Crystallographic studies of protein denaturation and renaturation. 2. Sodium dodecyl sulfate induced structural changes in triclinic lysozyme. *Biochemistry 16*, 1418−1424.